Acta Cryst. (1975). A31, 804

A Practical Method of Three-Dimensional Space-Group Analysis Using Convergent-Beam Electron Diffraction

BY P. GOODMAN

CSIRO, Division of Chemical Physics, P. O. Box 160, *Clayton, Victoria, Australia* 3168

(*Received* 23 *April* 1975; *accepted* 18 *June* 1975)

Symmetry rules are derived for relating the convergent-beam electron-diffraction pattern symmetries to the three-dimensional symmetry of the structure. These rules are applied to a study of 2*M* biotite. As a result the space group is determined as *C*2, or number 5 in *International Tables for X-ray Crystallography*, whereas it was previously held, in the absence of accurate data, to belong to *C*2/*c* or number 15. In addition, a method is described for uniquely determining the centrosymmetry of a crystal independently of space group, hence resolving the ambiguity between a centre of symmetry and a twofold axis present when approximations to dynamic electron scattering are used which take into account only the symmetry of the projection.

PART 1

Introduction

We are concerned in part 1 to give the symmetry relationship expected within the convergent-beam electron-diffraction pattern from a parallel-sided crystal, together with referenced derivations, and in part 2 to test these relationships and to demonstrate a practical approach to space-group analysis by means of a study of biotite.

As an introduction we mention the two most obvious aspects of symmetry in electron diffraction which lead to readily observable phenomena and which suitably illustrate the difference between X-ray and electron diffraction data in this respect:

(*a*) *The break-down of Friedel's law*

This has been stated in various ways (*e. g.* Miyake & Uyeda, 1955; Goodman & Lehmpfuhl, 1968; Tanaka & Lehmpfuhl, 1972), in reference to scattering from a non-centrosymmetric structure. However, in spite of this work there does not appear to be any hitherto published criterion for distinguishing centro- and non-centrosymmetric crystals in three dimensions; in this regard experimental technique has been ahead of tabulation.

(*b*) *Crystal boundaries*

The symmetries of the boundaries will naturally influence the symmetry of the pattern. This is because in dynamical scattering it is the symmetry of the crystal, and not that of the unit cell, which is operative, and the unit-cell symmetry which is of interest to the structure analyst can be derived from the pattern when the influence of the boundaries is taken into account. For a plane-parallel plate crystal this influence may be of three types:

(i) Termination of the structure after a non-integral number of unit cells (*e. g.* Lynch, 1971; Goodman & Moodie, 1974).

(ii) Termination of the structure after an integral number of unit cells, but with boundaries occurring so as to give a symmetry lower than the infinite structure (example: MoO_3).

(iii) Asymmetry arising from inclination of the incident beam to the surface normal (Goodman, 1974).

These two phenomena provided the initial suggestion that a practical and unequivocal method of space-group analysis could be established. A full theoretical approach to the symmetry problem would involve group theory (see Tinnapple, 1975). However, at a less ambitious level we have approached the problem through individual space-group elements, and our theoretical reference is to Moodie (1972). Work on similar lines, but with a different theoretical and experimental background, is being pursued by J. Steeds and colleagues (*e. g.* Steeds, Tatlock & Hampson, 1973). (It is also assumed in this discussion that we are dealing with a crystal free from faults, apart from the non-integral termination mentioned, although the practical problem of dealing with faults and curvature is mentioned in part 2. The soluble problem of crystals with horizontal stacking faults is discussed elsewhere and is outside the scope of this publication.)

Use of the projection approximation

In an earlier investigation (Goodman & Lehmpfuhl, 1968) we were content to show that a structure which was polar in projection displayed an asymmetry in the relationships of the *hk*0 diffracted intensities, and to show that the 000 pattern retained a centre of symmetry as predicted by the reciprocity theorem in the projection or zero-layer-interaction approximation. The projection approximation is that approximation which includes interactions only of, say, the *hk*0 reflexions of an [001] zone pattern, and is equivalent to considering the scattering from a crystal potential which has been averaged over one of its dimensions. It can therefore incorporate only the symmetries of the two-dimensional projection group and its accuracy is limited by the magnitude of interaction present in-

volving *hkl* ($l \neq 0$) reflexions and by tilted boundary effects. The projection approximation seems reasonable when the *c* axis is short (say ≤ 10 Å) for high-voltage electrons, and it allows a very convenient interpretation. However, a difficulty arises in that there is experimentally no very clear point, in general, at which it can be said to hold to a given accuracy. This difficulty would be met in attempting structure analysis solely from the electron diffraction data. In this case it is unlikely that sufficient structural information would be available to allow a quantitative examination of the effects of symmetry. It therefore seems wiser to follow the procedures for three-dimensional analysis initially, and to deduce the two-dimensional symmetry of a projection as a second step. The three-dimensional symmetry rules differ from those of the projection approximation in that we no longer have a one-to-one correspondence apparent between crystal and pattern symmetries, but in spite of this they are no more difficult to apply.

Special points and trajectories

This section is included particularly for the benefit of those unfamiliar with convergent-beam work who might otherwise find the significance of certain lines and points of the pattern obscure, including the definition of a zone. We use 'Kossel pattern' for convenience, rather than the unwieldy name 'wide-angle convergent-beam pattern' to describe the pattern produced by a large incident convergent beam which allows the diffracted orders to overlap, since the geometry is similar to Kossel pattern geometry. A small defocus (placing the cross-over above or below the crystal) produces sufficient contrast to determine the orientation and approximate symmetry of the crystal planes. A series of such patterns taken with different crystal orientations allows relatively large sections of the Kossel pattern to be mapped as part of the surface of a sphere, whose radius equals the camera length. Alternatively, using an aperture somewhere between the source and the main lens, to restrict the angle of the incident cone of radiation, one can prevent overlapping of diffraction orders, and map out sections of intensity distribution (from a spherical surface) contributed to by one order, *i. e.* the Kossel–Möllenstedt pattern. Manipulation of a Kossel–Möllenstedt aperture allows particular points in an *n*-beam interaction pattern to be located within a certain angular range without mechanical adjustment of the crystal. The idealized *Kossel lines* represent the trajectories of zero excitation error, and occur experimentally roughly at the centre of the line contrast. In scattering from the $\{hkl\}$ set of planes, both *hkl* and $\bar{h}\bar{k}\bar{l}$ reflexions are excited, leading to the appearance of a pair of parallel Kossel lines forming a '*Kossel band*'. For symmetry study we need to find a zone. As a working definition, a *zone* occurs whenever a reasonably strong pair of Kossel lines is crossed by at least one other pair (and will usually entail at least two, or three, other pairs). In this case, the intersection of the central lines of the crossing Kossel bands is unique, and called here the *centre of the zone.*

In the apertured Kossel–Möllenstedt pattern, each *hkl* diffraction order has a central line (the trace of $\zeta = 0$), and at a zone setting it has a *central point* given by the perpendicular intersection of this (Kossel) line with a second line drawn from the centre of the zone parallel to the *hkl* scattering vector. The central *line* and *point* are special in the symmetry of the intensity distribution, as a consequence of the reciprocity theorem; the second intersecting line will be a special symmetry line if it is parallel to a suitable crystal axis. For the 000 distribution there is a set of special lines, corresponding to the set of intersecting central lines of the Kossel bands, and its centre point is the centre of the zone. These definitions are necessary so that we can describe the experimental analysis without ambiguity.

Symmetries introduced by reciprocity

Diffraction symmetries can be conveniently considered in two groups: those determined directly, by the invariance of the crystal and the zone under consideration under a set of space-group operations, and those introduced by reciprocity. Since the latter symmetries are the less obvious and cause the most trouble in communicating results, they are described in more detail.

The reciprocity theorem has been described in terms of the Ewald construction by Moodie (1972). In this construction only the two beams of interest (in an *n*-beam situation) are shown, namely the incident and one scattered beam. The reciprocal diagram is obtained by reflecting the original diagram across the scattering vector, and according to the theorem represents an equivalent scattering path. If we regard the two beams of each diagram as input and output beams, reciprocity involves sending an input beam back along the original output path so that it strikes the reverse side of the crystal. Direct access to this configuration experimentally therefore involves rotating the crystal through 180°. Furthermore, the equivalence of this reciprocal configuration to the original or incident configuration is independent of any symmetry and holds for $P1$. For these reasons the first symmetry group to give accessible and useful pattern symmetry (*i.e.* accessible to practical convergent-beam diffraction) is $P\bar{1}$.

Translational symmetries

The convergent-beam (or Kossel–Möllenstedt) pattern consists of a set of *hkl* non-overlapping discs of intensity (for a diagram illustrating the formation of the pattern, see, Goodman, 1971). Each disc contains a two-dimensional rocking curve of the crystal, in which incident angular coordinates are transformed into *x*–*y* coordinates. These discs are disposed relatively on the observation plane with the geometry of the diffraction

pattern. In describing the pattern symmetry as a whole, we have to consider simultaneously the geometry within the discs and the geometry of their relative distribution. Since the 000 disc and also its centre are unique (*i.e.* the pattern has an origin) it might be supposed that we only need to consider the point-group, or multiplicative, symmetries of the pattern. This is certainly true for the pattern as a whole. However, it is also useful to consider the symmetries *within* the *hkl* order, and this includes geometrical relationships between *hkl* and $\bar{h}\bar{k}\bar{l}$ discs of the pattern. The most important example of this arises in the case of an isolated centre of symmetry.

(i) *Centre of symmetry*

Derivation of the pattern symmetry for a crystal with a centre of symmetry is given in Fig. 1. This demonstrates the translational relationship between *hkl* and $\bar{h}\bar{k}\bar{l}$ distributions. The translation distance is the length of the displacement $\mathbf{r}_{hkl}$ between the Kossel-line pair. This is the only symmetry in the pattern from a crystal of $P\bar{1}$ symmetry, or from a sufficiently arbitrary setting of any centrosymmetric crystal. No symmetry is introduced into the 000 distribution.

(ii) *Central horizontal rotation diads, twofold screw axes, glide planes, and mirror planes*

Central here means mid-way between the entrance and exit faces of the crystal along the zone-axis direction, which means in a regular structure (dependent of course on the positions of the boundaries) at $z=\frac{1}{2}$ in the unit cell for the [001] setting; horizontal means parallel to the plane of the diffraction pattern. A central horizontal rotation diad or twofold screw axis produces a mirror along any central line of an *hkl* distribution to which it is perpendicular. The construction for this proof is already given in another publication (Goodman, 1974). A central mirror or glide plane produces a centre of symmetry at the centre point of each *hkl* distribution. The construction for this proof is probably sufficiently obvious, following the method in Fig. 1. The condition of a central mirror plane has relevance to the projection approximation, since this is a condition imposed by this approximation. The disappearance of the centres of inversion from the *hkl* distributions can therefore be used as an experimental test of the breakdown of this approximation.

The results for the horizontal space-group elements are shown diagramatically in Fig. 2. The same rules apply to the 000 distribution as to the other orders for these elements.

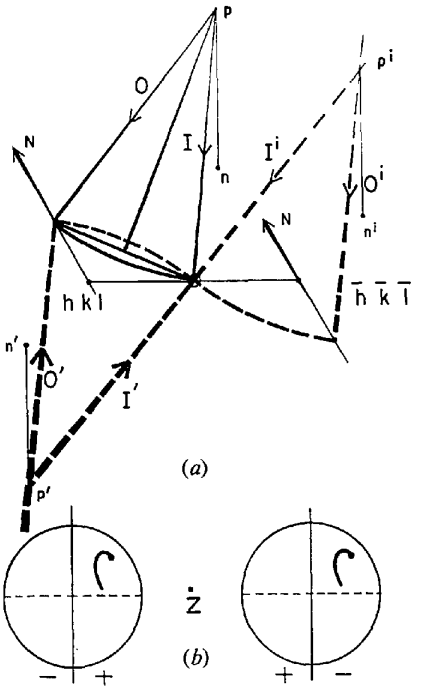

Fig. 1. (*a*) Ewald construction, showing the relationship between *hkl* and $\bar{h}\bar{k}\bar{l}$ reflexions in a centrosymmetric structure. *p*, *p'*, and p^i, represent the centres of Ewald spheres of the incident, reciprocal, and reciprocal-inverted diagram. The relationship between the incident and reciprocal diagrams is given by the reciprocity theorem and described by Moodie (1972). The inversion through the origin is an operation under which the scattering diagram is invariant under centrosymmetry. The incident diagram is drawn in a full line, the reciprocal diagram and its inversion in a dashed line. *I* and *O* are used to indicate input and output beams. *N* the surface normal and *n* the base of the perpendiculars dropped from *p* to the horizontal plane. (*b*) The translational relationship between *hkl* and $\bar{h}\bar{k}\bar{l}$ imposed on the convergent-beam distributions by a centre of symmetry, when these reflexions are separately satisfied, is shown here. This follows from the construction of (*a*). + and − indicate the sign of excitation error; the full line is the central Kossel line (see text).

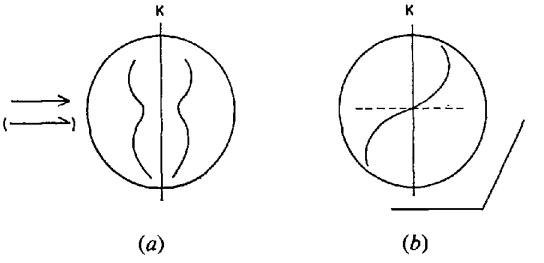

Fig. 2. The symmetries imposed upon an $\bar{h}kl$ distribution under the influence of horizontal symmetry elements. The vertical bisecting line (*K*) represents the central Kossel line (see text). (*a*) A central horizontal rotation diad or twofold screw axis imposes a mirror line when it is perpendicular to the central Kossel line. (*b*) A central horizontal mirror plane (shown) or glide plane imposes a centre of inversion on the *hkl* distribution.

Vertical symmetry elements

Vertical here means in the direction of or parallel to the zone axis. Symmetries imposed by vertical elements are direct, *i.e.* independent of reciprocity. Hence, *n*-fold rotation axes parallel to a zone impose an *n*-fold rotation symmetry upon the diffraction pattern, relat-

ing the *hk*0 intensity distributions of the zone. The 000 distribution will have *n*-fold rotational symmetry about its centre.

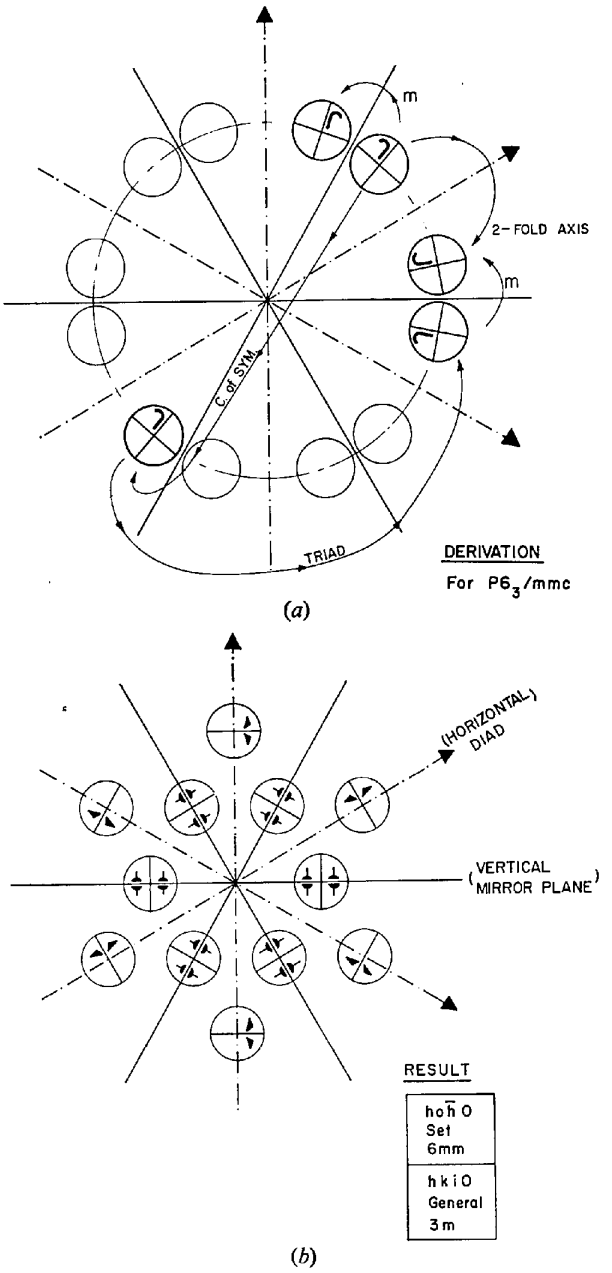

Fig. 3. Derivation of the pattern symmetry for the [001] zone axis for the space-group $P6_3/mmc$. This example illustrates the influence of several of the space-group elements discussed in the text. Each *hkl* disc is divided by the intersecting central line and scattering vector as discussed in the text. Since the central points of each disc could not be displayed in a single convergent-beam pattern, the diagrams represent a hypothetical pattern, with all the relevant information which would be assembled from a group of convergent-beam patterns. (*a*) Derivation of symmetries from vertical mirror planes (*m*), horizontal twofold axes (arrow-head), triad, and centre of symmetry. (*b*) Resultant symmetry shown for two sets of reflexions belonging to different sub-set symmetries.

Vertical mirror planes, and vertical glide planes with no *z* component of translation (with *z* parallel to the surface normal), will impose mirror lines on the zone-axis pattern as a whole, which will run through the zone centre on the 000 distribution and bisect certain *hk*0 distributions in the Kossel–Möllenstedt pattern.

Vertical *n*-fold screw axes and vertical glide planes with a *z* component introduce no additional symmetries into the diffracted intensities (*i.e.* as distinct from those introduced into the Kossel-line geometry), the corresponding rotation and mirror symmetries appearing only as the projection approximation is approached.

The above set of restricted conditions is arrived at by considering only those space-group operations which turn the crystal and the zone under consideration back into itself or itself translated parallel to the infinitely extending boundaries. An example of the derivation of a pattern symmetry from these rules for a particular space-group and zone is given in Fig. 3. The use made of two-dimensional point-group symbols in the accompanying table to describe pattern symmetries is convenient, but should not be confused with their use to describe unit-cell symmetries. The example is not necessarily of practical interest, since we are much more likely to work back from specific symmetry elements and from a series of patterns, than from theoretically correct zone symmetries, which may not always be detectable. Techniques can then be employed to amplify specific effects.

Use of the parallel-plate boundary conditions

Influence of the third dimension of the crystal is introduced into the pattern by wave propagation. As has been shown (Goodman, 1974), this influence can arise through tilted boundaries as well as through a long *c* axis. Thus three-dimensional interactions may be introduced visibly into a pattern by a sufficient tilt, regardless of the unit-cell size. This phenomenon finds practical application in analysis. Zones which are located at a high tilt have the boundary symmetry superimposed on them. A tilted plate has only two symmetries with respect to the zone, namely a horizontal rotation diad, and a centre of symmetry. Provided these symmetries are also present in the crystal structure they will be detected in the diffraction pattern. This is particularly valuable in allowing centrosymmetry to be tested for separately, and in the presence of other symmetry elements. Without this boundary condition, for example with a spherical crystal, analysis of the more highly symmetric groups would actually be more difficult.

PART 2

A. Tests with MgO

MgO has a known simple centrosymmetric structure. At the [111] setting a (100)-faced plate has the known reduced symmetry of the tilted plate with respect to

the zone axis. It therefore provides a good test for the derivation of Fig. 1 for centre of symmetry. Already evidence has been provided (Goodman, 1974) which tests the behaviour derived above for a horizontal rotation diad. In Fig. 4 of that reference the $02\bar{2}$ distribution has a mirror symmetry about its centre line because this line is perpendicular to the rotation diad of the crystal, and Fig. 5(*a*) and (*b*) of that reference provide the proof. This test is not a specific test for a centre of symmetry, however. For this purpose it is better to choose a reflexion pair whose centre lines are not perpendicular to the diad, and which therefore lack mirror symmetry. This makes the task of looking for a translational relationship between *hkl* and $\bar{h}\bar{k}\bar{l}$ distributions easier (and the result more convincing: even with a mirror line the distributions should still lack a centre of symmetry owing to the boundary conditions, so that a translation could still be distinguished from a twofold rotational relationship, through not from a mirror relationship). In Fig. 4 of the present paper a pair of patterns are shown in which the $20\bar{2}$ and $\bar{2}02$ reflexions, respectively, are satisfied. Owing to the lack of mirror symmetry, the subsidiary maxima in the 202-indexed beams identify a top and bottom to the distributions. A square bracket, coupling the first fringe on one side with the second fringe on the other as fringes of approximately of equal intensity, helps one to identify the change between Figs. 4(*a*) and (*b*) as a *translation* of intensity pattern.

B. Space-group determination of a biotite sample

Cleaved crystals from a mineral biotite sample were mounted in the Elminskop 1 universal tilt stage, which was copied from the Mills & Moodie (1968) design. This stage allows the specimen to be examined in the back focal plane of the objective, thus allowing convergent-beam diffraction to be carried out conveniently and with full use of the goniometer. There were many thin regions of crystal which readily gave clear convergent-beam patterns, but which suffered from crystal curvature, and from inclusions or bubbles on a fine scale. These crystal defects limited the experimental accuracy obtainable from the thin regions. However, much useful data could be obtained from these regions with little trouble. When specific points requiring higher accuracy arose, patterns were taken from much thicker regions, which were essentially flat, and as a consequence the pattern detail was not dependent on the precise focusing of the beam on the crystal. Bubble contrast still appeared but was easily distinguished from the pattern detail. Furthermore in diffracting from thicker regions certain effects of dynamic scattering useful in the analysis were amplified.

Three types of pattern were used. Both Kossel patterns (wide-angle convergent-beam patterns) and convergent-beam diffraction patterns were used to provide the main symmetry data, but also normal point patterns obtained by focusing the beam on the photographic plate with condenser 2 were used to identify diffraction spacings, and systematic absences, to monitor crystal rotations through large angles, and particularly to measure the *c* spacing, a measurement which required a high crystal inclination to the beam. The experimental procedure was as follows:

(i) A thin crystal was oriented with the goniometer into the [001] setting. This setting was identified by reason of being the principal zone, obtained with the crystal flake approximately horizontal, which gave the most closely spaced pseudo-hexagonal, or centred, diffraction pattern. This identification was confirmed by later measurements. The Kossel pattern at [001] showed a rectangular symmetry (see *A* in Fig. 5), showing that the crystal probably belonged to either the orthorhombic or monoclinic systems. By inserting an aperture a Kossel–Möllenstedt pattern at the zone was obtained (see Fig. 6) which showed centring ($h+k=2n$) and approximately *cmm* (No. 9) two-dimensional space-group symmetry. (Note: we can assess the two-dimensional group approximately in a very direct way because of the one-to-one correspondence of symmetry in the projection approximation.)

(ii) The next step was to take Kossel–Möllenstedt patterns above and below the main [001] zone. The nearest minor zone below [001] (reached by rotation about **a***) has an inclined intersection (see *B* in Fig. 5). These inclined (to **a***) lines were tentatively indexed as $\bar{3}92$, $3\bar{9}\bar{2}$, although the analysis is not dependent upon correct indexing. The pair of Kossel–Möllenstedt patterns shown in Fig. 7, taken either side of the [001] zone exciting respectively $\bar{3}92$ and $3\bar{9}\bar{2}$ in two separate four-beam excitations together with the 200 reflexion, established the fact that the inclination was *mirrored* across the a^* axis and not rotated around the zone. This ruled out the possibility of a vertical twofold axis and hence ruled out the orthorhombic space groups as a possibility.

(iii) The space group was then assumed to be monoclinic or triclinic. However, the [001] projection space group is either *cmm* or *c*1*m*. This would leave open the possibility of space groups 5, 8, 9, 12 and 15. Although the actual symmetry of the zone pattern (Fig. 6) is only 1*m* and not 2*mm* because of the clear inequality of the 200 and $\bar{2}00$ distributions, we cannot immediately rule out the two-dimensional space group *cmm* for the projection, since the one-to-one correspondence between pattern and unit-cell symmetry only holds within the applicability of the projection approximation, or in other words when upper-layer interactions can be ignored. Some tests of the projection approximation were carried out in the vicinity of [001]. Reflexions were excited whose scattering vectors lay along no special crystal axes. Two examples are shown in Fig. 8, one with a small aperture close to 001, the other with a larger aperture near the neighbouring zone $\bar{2}03$. In these pictures, the excited reflexion is encircled and the centre of the *hkl* distribution indicated with a dot. It can be seen that to a reasonable accuracy these distributions

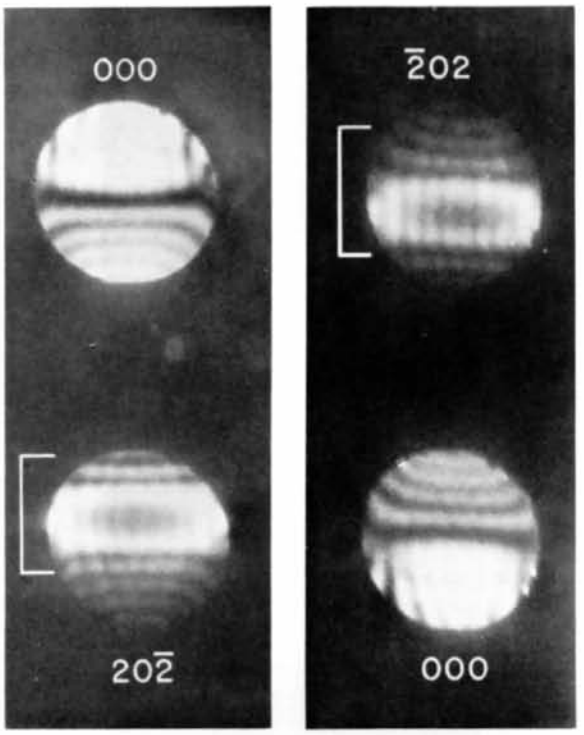

(*a*) (*b*)

Fig. 4. A pair of diffraction patterns taken satisfying (*a*) $20\bar{2}$ and (*b*) $\bar{2}02$ reflexions of MgO, near the [111] zone axis, using a plate crystal with (100) faces. The rotation axis of the crystal (giving the rotation from [001] to [111] zones) is at an angle of 60° to the central line of the distributions, which means that these have no mirror-line symmetry. Hence subsidiary maxima are stronger on one side than the other side of the central line, by a factor of at least two. Subsidiary fringes of equal intensity are coupled by a square bracket, demonstrating that the asymmetric distribution is *translated* and not rotated in moving from the *hkl* and the $\bar{h}\bar{k}l$ excitation.

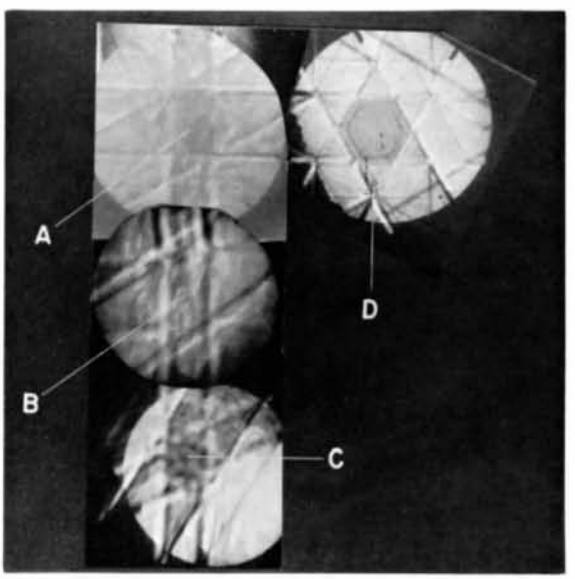

Fig. 5. A composite picture composed from four Kossel patterns. *A* is the [00*l*] or principal pattern; *B* and *C* are neighbouring [0*kl*] zones; and *D* is the neighbouring [*h*0*l*] zone. These zones are referred to in the text, and are used for the following convergent-beam diffraction pictures.

To face p. 808

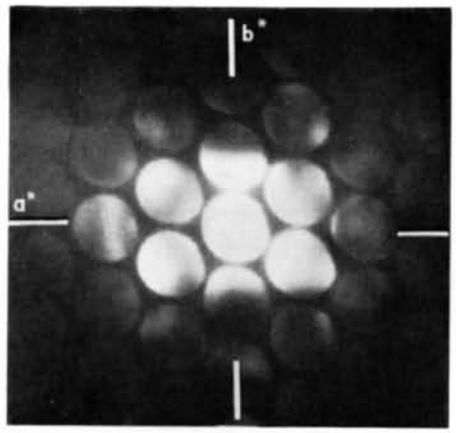

(*a*)

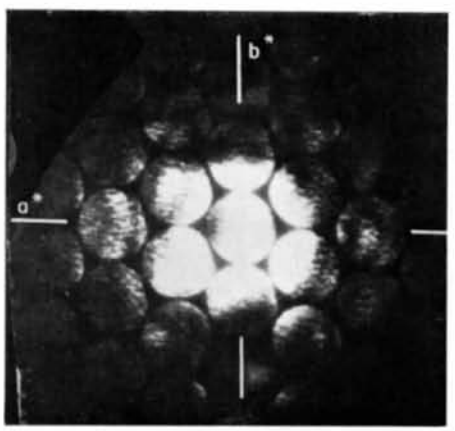

(*b*)

Fig. 6. Kossel–Möllenstedt patterns taken from the [001] zone: (*a*) is the picture obtained at exact focus; (*b*) is obtained by going two fine stops on the objective lens control away from focus. In spite of the dense bubble contrast the main symmetry features of the zone remain in evidence. Note the asymmetry between 200 and $\bar{2}00$ distributions, resulting in a pattern symmetry of $1m$.

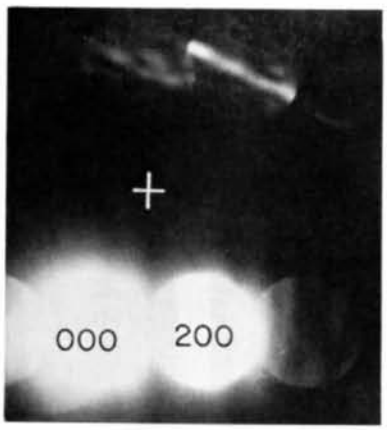

(*a*)

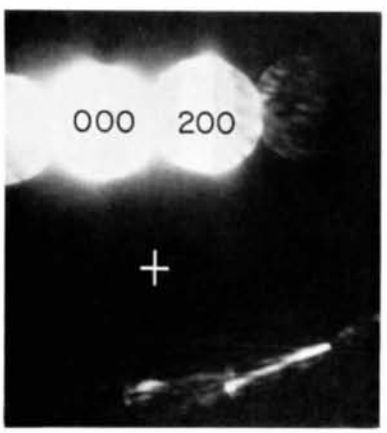

(*b*)

Fig. 7. A pair of Kossel–Möllenstedt patterns taken (*a*) above and (*b*) below the [001] zone which is indicated by a cross (see region *B* of Fig. 5). These show a reflexion of the inclined intersection across the a^* axis, rather than a rotation around the [001] zone.

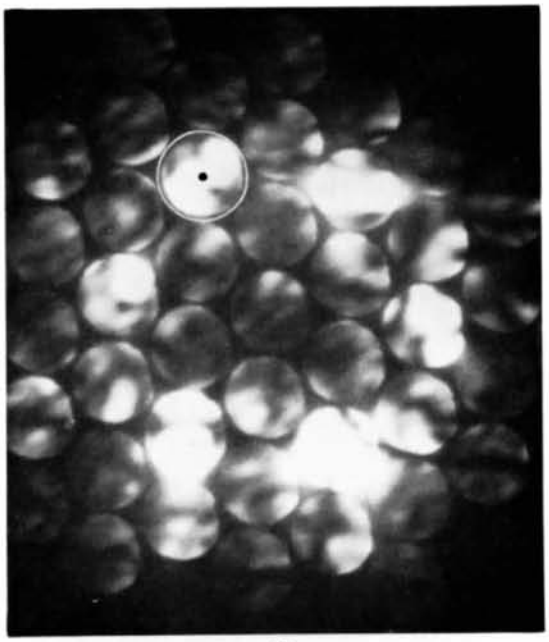

(*a*)

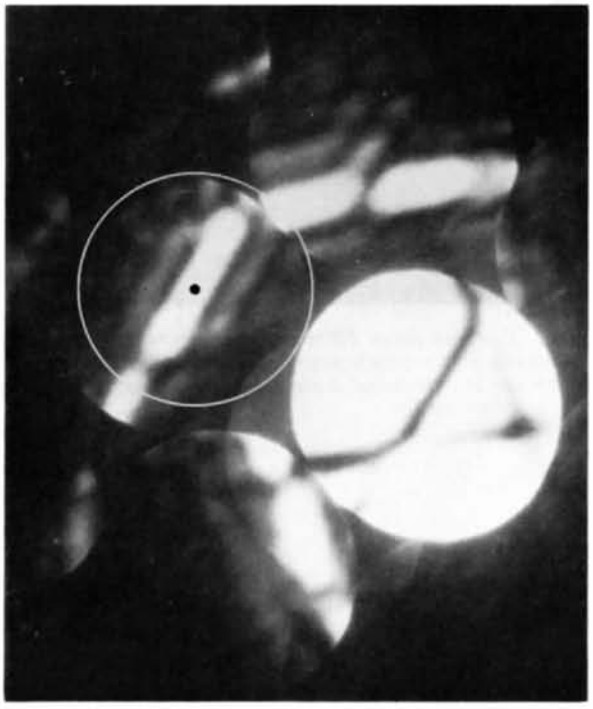

(*b*)

Fig. 8. Two Kossel–Möllenstedt patterns taken so as to satisfy a general reflexion, *i.e.* a reflexion with a scattering vector parallel to no principal crystal axis. (*a*) Close to the [001] zone, using a small aperture. Encircled reflexion shows a centrosymmetric *S* pattern. (*b*) Close to the [$\bar{2}$03] zone where a large aperture could be used. Encircled reflexion again shows an inversion symmetry about the indicated reflexion centre.

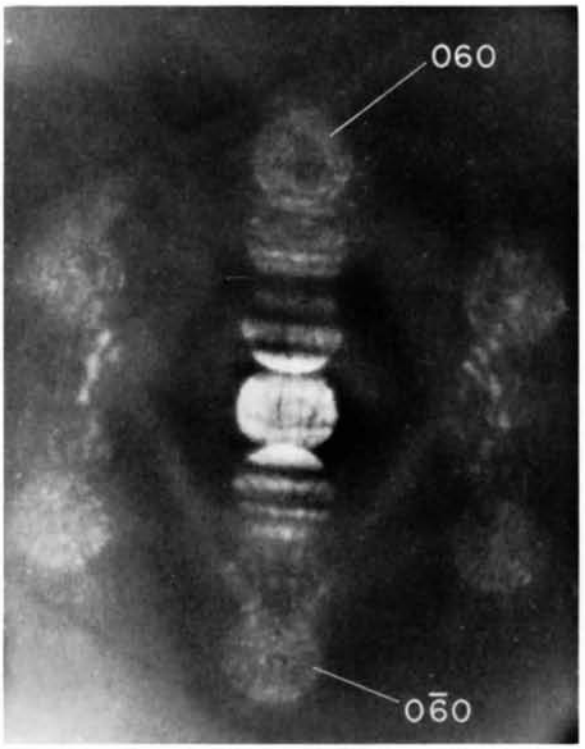

Fig. 9. Kossel–Möllenstedt pattern taken at the [$\bar{2}$03] zone. This pattern clearly indicates the absence of any mirror or glide plane parallel to **a*** (see text), *i.e.* parallel to the horizontal axis of the picture.

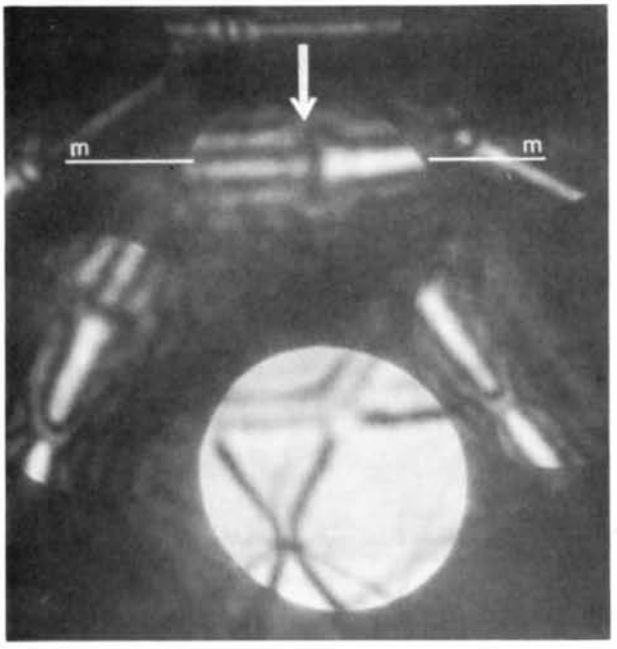

Fig. 10. Pattern taken near the [$\bar{2}$03] zone in which a reflexion is satisfied with a scattering vector parallel to a supposed horizontal twofold axis (indicated by arrow). The apparent mirror symmetry seen in this distribution about the indicated centre line tends to confirm the twofold axis.

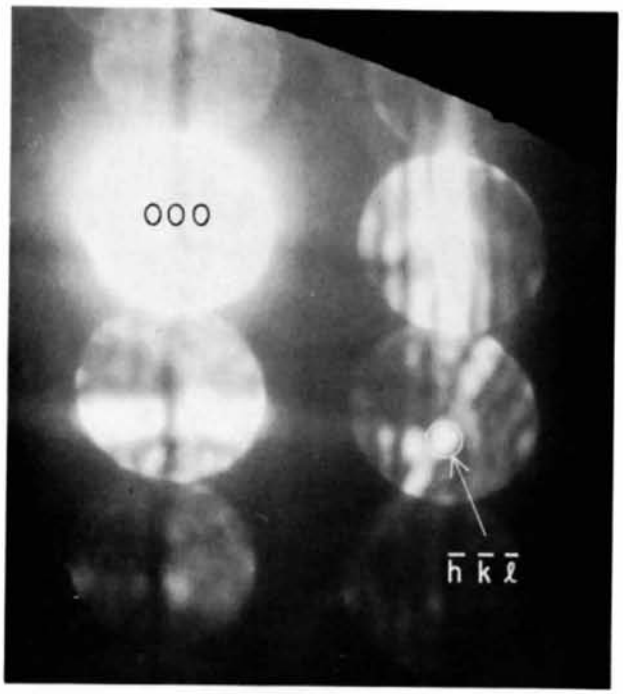

(*a*)

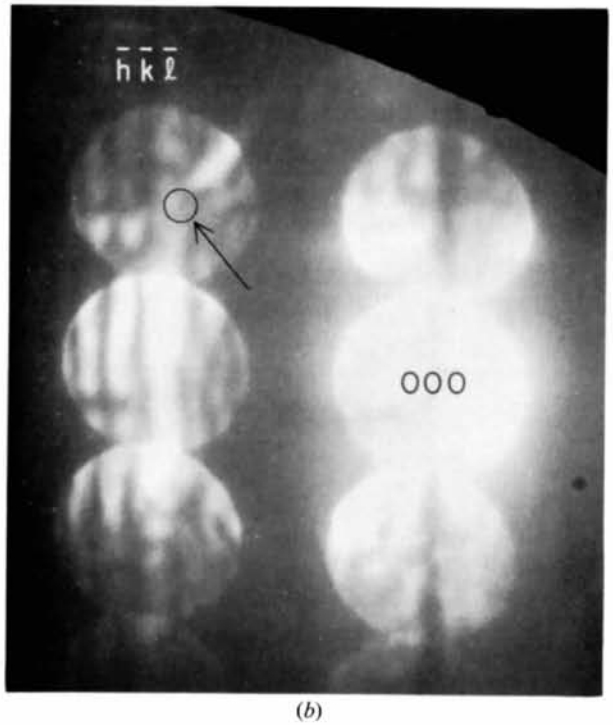

(*b*)

Fig. 11. A pair of Kossel–Möllenstedt pictures taken at an unidentified zone approximately 40° in rotation from [001]. In each picture an arrow indicates the encircled centre of a satisfied reflexion; in one case the hkl, and in the other the $\bar{h}\bar{k}\bar{l}$ reflexion, is satisfied. A lack of inversion symmetry within each reflexion (contrast with Fig. 8), and an approximate translation of some of the intensity features between pictures may be observed.

Fig. 12. Focused point diffraction pattern with the incident beam at a high inclination to the c axis, so that the projected c spacing and projected β angle can be measured to identify the polytype as $2M$.

have a centre of inversion about their centres. This indicates that the projection approximation is holding up sufficiently well for us to identify the projection symmetry group as $c1m$, thus leaving space groups 5, 8 and 9 as possibilities. (Note: this test establishes *either* the validity of the projection approximation, *or* the presence of a central mirror/glide plane. In either case the interpretation of the zone pattern given is justified.)

(iv) The next step was to rotate the crystal about **b***, to the [203] zone (*D* in Fig. 5) in order to check for glide and mirror planes and twofold axes. For the space groups considered glide or mirror planes may exist parallel to **a***, *i.e.*, the mirror line and glide lines of the two-dimensional space group may or may not correspond to mirror or glide planes in three dimensions. For this purpose a Kossel–Möllenstedt aperture was placed at the centre of the hexagonal Kossel pattern which defines the $\bar{2}03$ zone. A crystal was chosen to be as thick as possible consistent with a reasonable exposure time, in order to obtain the greatest sensitivity. The resulting pattern in Fig. 9 clearly demonstrates that no vertical mirror or glide plane exists in the unit cell. The 020, $0\bar{2}0$ distributions are perceptibly different, the 040, $0\bar{4}0$ distributions are completely different, one of them being practically of zero intensity, while the 060, $0\bar{6}0$ distributions have a different shape, one being full and the other having a doughnut appearance. These asymmetries are clearly not attributable to experimental error and rule out the centrosymmetric groups 12 and 15 (as was already suggested in the previous paragraph from the deduced two-dimensional space group), and the non-centrosymmetric groups 8 and 9. At this stage we have deduced that if the system is monoclinic, the correct space group is number 5 ($C2$).

(v) The final step in this analysis is to establish as conclusively as possible, whether the system is monoclinic as distinct from triclinic. In the absence of mirror or glide planes the monoclinic system is characterized by horizontal twofold axes. For this test several patterns were taken in which reflexions were excited whose scattering vector lay parallel to the supposed twofold axes, *i.e.*, whose centre line would be perpendicular to the axes. Thin crystal regions were used in order to obtain a clear view of several subsidiary fringes, and for the same reason a large aperture was chosen. The results show that these reflexions have a central mirror line in their intensity distribution to quite a reasonable accuracy. The presence of a mirror line is made more striking when these distributions are compared with other distributions having scattering vectors in other directions (see Fig. 10). It is concluded that to a reasonably high accuracy the correct space group is $C2$, monoclinic, rather than $P1$. If the need ever arose to distinguish between these groups with higher precision this study could be pursued with patterns from thicker crystals.

(vi) The next experiment was an independent test for centrosymmetry. This test may appear academic at this stage since Fig. 9 establishes fairly conclusively that the structure is noncentrosymmetric. However, the opportunity was taken to implement the test for centrosymmetry described in part 1, since it is desirable to accumulate information on the degree to which the hkl to $\bar{h}\bar{k}\bar{l}$ translational relationship can be observed in various structures. For this purpose the crystal was rotated away from the [001] zone, about an arbitrary axis, by an angle approaching 40°, when it became apparent by the disappearance of a centre of inversion from the hkl distributions that the projection approximation was no longer holding, owing to the inclined boundaries. A high-angle zone was located of unknown index. It can be seen from Fig. 11, in which the centres of the satisfied reflexions are indicated, that there is a complete lack of inversion symmetry (contrast with Fig. 8) in these reflexions, and that the distributions have something of the shape of a boomerang. It can also be seen that there is a tendency towards a translational relationship between the satisfied hkl and $\bar{h}\bar{k}\bar{l}$ distributions, but that the relationship is not complete, most noticeable being the disappearance of the strong central intensity in one case. We conclude from this that the translational component arises from the centrosymmetry of the boundaries, and that the difference between the two distributions arises from the lack of centre in the crystal structure, apart from the experimental error involved from crystal curvature.

(vii) Up till now no reference has been made to the X-ray-determined structure. It now becomes interesting to compare our results, and it is first necessary to measure the c spacing in order to identify the polytype positively. A point pattern was taken from a crystal tilted at a high inclination to the beam, after rotation around an axis approximately parallel to **a*** (see Fig. 12). The crystal shape transform was cut at sufficiently low angle to display the projected c spacing, and after measuring the projected β angle the c spacing was calculated as $\simeq 20$ Å, with $\beta \simeq 95°$. This corresponds to $2M$ biotite (Hendricks & Jefferson, 1939). However, the space group allocated from the X-ray data is number 15, or $C2/c$, but the discrepancy is not too surprising since X-ray investigation of biotite, and the micas in general, is extremely difficult (see, for example, Deer, Howie & Zussman, 1965). It is also possible that samples of $2M$ biotite from different sources have slightly different structures, but the main point to be made is that the electron diffraction method offers a far clearer and more direct answer to the space-group question for this class of mineral.

The author wishes to acknowledge the assistance given him by Mr A. F. Moodie and Dr John Steeds, who provided, through discussions and correspondence, the stimulus to develop the present methods.

References

Deer, W. A., Howie, R. A. & Zussman, J. (1965). *Rock-Forming Minerals*, p. 55. London: Longmans.

GOODMAN, P. (1974). *Nature, Lond.* **251**, 698–701.
GOODMAN, P. (1971). *Encyclopaedic Dictionary of Physics* Suppl. Vol. 4, pp. 65–69. Oxford: Pergamon Press.
GOODMAN, P. & LEHMPFUHL, G. (1968). *Acta Cryst.* A**24**, 339–347.
GOODMAN, P. & MOODIE, A. F. (1974). *Acta Cryst.* A**30**, 280–290.
HENDRICKS, S. B. & JEFFERSON, M. E. (1939). *Amer. Min.* **24**, 729–771.
LYNCH, D. F. (1971). *Acta Cryst.* A**27**, 399–407.
MILLS, J. C. & MOODIE, A. F. (1968). *Rev. Sci. Instrum.* **39** 962–969.
MIYAKE, S. & UYEDA, R. (1955). *Acta Cryst.* **8**, 335–342.
MOODIE, A. F. (1972). *Z. Naturforsch.* **27a**, 437–440.
STEEDS, J. W., TATLOCK, G. J., & HAMPSON, J. (1973). *Nature, Lond.* **241**, 435–437.
TANAKA, M. & LEHMPFUHL, G. (1972). *Acta Cryst.* A**28**, S202.
TINNAPPEL, A. (1975). Doctorate Thesis. Berlin Technical Univ.

Acta Cryst. (1975). A**31**, 810

Thermal Contraction in NH_4IO_3 and its Significance with Respect to the Phase Transition

BY K. VISWANATHAN AND E. SALJE

Mineralogical Institute of Technical University, Welfengarten 1, *Hannover, Germany (BRD)*

(*Received* 5 *May* 1975; *accepted* 12 *May* 1975)

NH_4IO_3 shows an abrupt contraction in the direction of spontaneous polarization at 82 °C. This anomaly is accompanied by changes in the optical properties and phonon spectra, which were also studied at different pressures. On the basis of the lattice parameters and Raman spectra a probable mechanism is suggested for the phase transition.

Introduction

Iodates with large ions such as K, Rb and Cs, possess perovskite-like structures with distorted octahedral coordination for I. Those with smaller ions like H, Li and Na show other structures, in which the typical octahedral framework of the perovskite is lacking. The latter are characterized by pyramidal IO_3^- ions. The structure of NH_4IO_3 (Keve, Abrahams & Bernstein, 1971) is noteworthy because it shows the characteristics of both types, namely pyramidal IO_3^- ions occur in a distorted perovskite-like structure, thereby giving rise to interesting physical properties. Some of these were studied by Crane, Bergman & Glass (1969) and Salje (1974*b*) who observed a phase transition at 85 °C. The aim of this study is to understand the nature of the transformation and to test if NH_4IO_3 is really ferroelastic as suggested by Keve *et al.* (1971).

Experimental

The phase transformation of NH_4IO_3 was studied by X-ray, optical and Raman spectroscopic methods at different temperatures and pressures. The variation of the lattice constants with temperature was studied with a focusing Guinier-type camera. The orientation relations between the different lattices were studied with a precession camera by heating single crystals on an iron–constantan thermoelement to about 100 °C.

The refractive index n_β was measured at room temperature by the immersion method and the birefringence with a Zeiss compensator. The optical orientation and the optic axial angle were determined with an universal stage which could be heated to about 120 °C. The transition temperature could be determined accurately by measuring the changes in the birefringence with a laser beam as source of light in a conoscopic arrangement and a photomultiplier to measure the changes in the intensity of the transmitted light.

The dependence of the phonon spectra on hydrostatic and uniaxial pressure and temperature was determined in a Raman experiment described earlier (Salje, 1974*a*). Hydrostatic pressures up to 1·5 kbar were produced in a heatable steel vessel with corundum windows and with argon as the pressure medium. Higher pressures up to 20 kbar were applied in a piston cylinder apparatus with windows made of corundum, mounted in a small furnace. Uniaxial pressures were obtained by keeping the crystal in a heatable forceps. The pressure was varied by tightening a screw.

Results

NH_4IO_3 shows two phase transitions, one at 82 °C and the other at about 115 °C. At room temperature the following optical parameters have been observed:

$$n_\alpha = 1{\cdot}777;\ n_\beta = 1{\cdot}785;\ n_\gamma = 1{\cdot}826;\ 2V = 48{\cdot}2°.$$

The orientation of the indicatrix is: n_α, n_β and n_γ parallel to [100], [010], and [001] respectively. The optic character is positive. The optic axial angle $2V$ increased gradually on heating to a value 60·2° just